Comparative Analysis of Frequency-Domain Filters for Speckle Reduction in PolSAR Imagery

Bhakti Talele
Carnegie Mellon University, Pittsburgh, Pennsylvania, United States

Sai Gurav
University of Southern California, Los Angeles, California, United States

Avinash Dhiran
University of Twente, Enscede, Overijssels, Netherlands

Aarya Shinde
University of Mumbai, Mumbai, Maharashtra, India

Varsha Turkar
Thakur Shyamnarayan Engineering College, Mumbai, Maharashtra, India

Yogesh Agarwadkar
InfiCorridor Solutions Pvt. Ltd. Mumbai, Maharashtra, India

Mugdha Agarwadkar
A.P Shah Institute of Technology, Mumbai, Maharashtra, India

ABSTRACT
In remote sensing, high-quality image data is crucial for effective analysis and interpretation. This study focuses on analyzing the impact of image quality by applying various frequency-domain filters like Gaussian, Butterworth, Chebyshev, Ideal, Elliptic, Laplacian, Extended Adaptive Wiener, Logarithmic and Homomorphic filter on the T3 components of SAR imagery. A quantitative analysis of image quality was carried out using metrics such as the Coefficient of Variation (CV), Signal-to-Noise Ratio (SNR), Equivalent Number of Looks (ENL), Structural Similarity Index Measure (SSIM), and Peak Signal-to-Noise Ratio (PSNR). Compared to the traditionally used Lee Refined filter, the Extended Adaptive Wiener filter demonstrated improved SNR, PSNR, and SSIM, with only slight compromises in CV and ENL. While the Lee Refined filter maintained balanced performance, other frequency-domain filters tended to either over-smooth (e.g., Butterworth, Homomorphic) or underperform (e.g., Chebyshev, Elliptic, Gaussian, Ideal, Logarithmic). These findings highlight the Extended Adaptive Wiener filter as a promising approach for speckle reduction in PolSAR data, supporting improved clarity and structural preservation in remote sensing applications.

Keywords
Synthetic Aperture Radar (SAR), Frequency Domain Filtering, T3 Matrix Components, Image Quality Assessment, De-speckling, Extended Adaptive Wiener

1. INTRODUCTION
Remote sensing has become an essential tool in fields such as agriculture, urban planning, and environmental monitoring, providing detailed information about the Earth's surface under various conditions. However, the quality of remotely sensed images, particularly Synthetic Aperture Radar (SAR) imagery, is often compromised by speckle—granular patterns that obscure critical details. While speckle contains useful information, it complicates image interpretation, necessitating filtering for improved post-processing tasks like segmentation and classification (Ansari et al., 2020; Turkar et al., 2025).

Image quality refers to the ability of a filtered SAR image to retain essential structural and radiometric features while reducing speckle noise. It reflects how well a filtering technique preserves meaningful image content such as edges, point targets, and texture, without introducing artifacts or distorting the polarimetric and statistical properties of the data. High image quality supports accurate interpretation and enhances the performance of downstream tasks such as classification and feature extraction (Jain et al., 2020).

Various image enhancement techniques have been developed to improve visibility by emphasizing important features while suppressing less relevant information. These include spatial filtering, which modifies pixel values based on surrounding information, and transform domain filtering techniques using Fourier or wavelet transforms, which manipulate frequency components to reduce noise while maintaining structural integrity (Oliver and Quegan, 2004; Richards, 2013; Argenti et al., 2013).

Frequency domain techniques offer significant advantages in image processing, particularly for reducing speckle noise in Synthetic Aperture Radar (SAR) imagery. These methods leverage the frequency characteristics of images, enabling more effective noise management while preserving essential image details. Frequency domain methods such as wavelet transforms allow for the separation of high-frequency noise from image data, facilitating targeted noise reduction (Tondewad and Dale, 2023). Techniques like SAR−FDD utilize frequency decomposition to isolate noise by employing filters that specifically target high-frequency components, which are typically associated with speckle noise (Zhao et al., 2024). The application of frequency domain techniques has also been shown to enhance qualitative metrics such as Peak Signal-to-Noise Ratio (PSNR) and Structural Similarity Index (SSIM), indicating better visual quality and detail preservation. By

focusing on different frequency bands, these methods can adaptively reduce noise while maintaining edge and texture fidelity, which is crucial for accurate interpretation of SAR images (Mohan et al., 2016). Additionally, many frequency domain techniques are computationally efficient, making them suitable for real-time applications in SAR imagery, which is essential for timely data analysis (Kapil et al., 2015). However, while frequency domain techniques provide substantial benefits for speckle noise reduction, it is important to consider that they may require careful tuning of parameters to avoid over-smoothing, which can lead to the loss of critical image details, highlighting the need to balance noise reduction with detail preservation.

The evaluation of image quality is critical in determining the effectiveness of enhancement techniques. Key indices include the Coefficient of Variation (CV), Signal-to-Noise Ratio (SNR), Equivalent Number of Looks (ENL), Structural Similarity Index Measure (SSIM), and Peak Signal-to-Noise Ratio (PSNR) provide comprehensive assessment of perceived image quality (Kumar and Singh, 2019; Jiao and Dong, 2013; Jain et al., 2023).

In Polarimetric SAR (PolSAR) imagery, the T3 coherency matrix, comprising six unique elements (T11, T22, T33, T12, T13, and T23), is fundamental for representing target scattering properties, where T11, T22, and T33 are real-valued diagonal elements indicating the power of individual polarization channels, and T12, T13, and T23 are complex-valued off-diagonal elements capturing inter-channel correlations, making their preservation during speckle reduction critical for accurate target characterization and classification (Jain et al., 2024).

This study aims to systematically evaluate the performance of nine frequency domain filters on T3 components of image data. The selection includes Gaussian filters for edge-preserving smoothing, Butterworth filters for smooth frequency transitions, Chebyshev filters for precise frequency selection, and Elliptic filters for rapid transition with minimal ripple, and Ideal filters (Laghari et al., 2014; Ge et al., 2023; Achim et al., 2006). Additionally, specialized techniques such as Homomorphic filtering, Extended Adaptive Wiener filter, and Logarithmic filters have shown promise in addressing specific challenges in SAR image enhancement (Salehi et al., 2020; Kanoun et al., 2019; Moreira and Misra, 2013). Traditional approaches like Low-pass, Laplacian, and Lee refined filters continue to play crucial roles in noise reduction and feature enhancement (Hazarika et al., 2016; Geetha and Narayanan, 2015; Lee, 1981).

These filters are evaluated not only for their noise reduction capabilities but also for their alignment with fundamental principles of PolSAR speckle filtering (Lee et al., 1999), which emphasize retaining key polarimetric information such as phase and scattering behaviour to preserve the physical interpretation of targets, adapting to local image characteristics by allowing stronger smoothing in uniform regions while maintaining detail in complex areas, and ensuring that the filtered data remains statistically valid to avoid bias in subsequent analysis.

This study evaluates the performance of various frequency-domain filters against the widely used Lee Refined filter using multiple quantitative image quality metrics to identify which metrics best reflect perceptible improvements in PolSAR image quality. The objective is to optimize frequency-domain filters for speckle reduction in T3 matrix components to preserve critical polarimetric and structural information necessary for accurate target characterization. Traditional spatial-domain filters, though mature, often over smooth edges and blur fine details, limiting structural fidelity (Alam and Rai, 2022), whereas frequency-domain methods demonstrate superior ability to suppress noise while retaining edges and textures (Zhao et al., 2024). By implementing dynamic, component-specific parameter tuning, this work addresses the research gap in frequency-domain de-speckling of PolSAR coherency matrices, demonstrating improved image quality compared to benchmark spatial methods.

2. STUDY AREA AND DATASET

The SAR dataset used is the AIRSAR STK–MLC L-band image over Flevoland, Netherlands, covering 400 × 400 pixels. Flevoland's diverse agricultural, urban, and natural landscapes make it ideal for evaluating speckle reduction across land cover classes with statistical reliability. Additionally, point target image data is included for focused evaluation, as it better reveals filter performance in preserving edges, fine structures, and low-contrast regions, factors that full-scene averages may obscure. Earlier studies confirm point target imagery enables precise assessment of mean preservation, edge definition, target retention, and class separability (Masurkar et al., 2020; Del Frate et al., 2003).

3. RESEARCH METHODOLOGY

The study involves processing PolSAR data to obtain the T3 matrix components of SAR data, which represent the polarization states. These components are then utilized for further analysis and quality assessment. As shown in Fig. 1, the study employs nine frequency domain filters.

The filtering process is conducted for each combination of filter type by applying the selected filters to the diagonal elements of the T3 matrix components (T11, T22, and T33). This process involves computing the Fourier Transform of each component, applying the selected filter in the frequency domain, and performing an Inverse Fourier Transform to obtain the filtered image in the spatial domain.

The real and imaginary parts of the T12, T13, and T23 components are combined to form complex matrices as given in the eq. (1), (2), and (3). This process allows for a comprehensive representation of the polarization states within the Coherency T3 matrix.

$$T12 = T12real + j \cdot T12imag \quad (1)$$

$$T13 = T13real + j \cdot T13imag \quad (2)$$

$$T23 = T23real + j \cdot T23imag \quad (3)$$

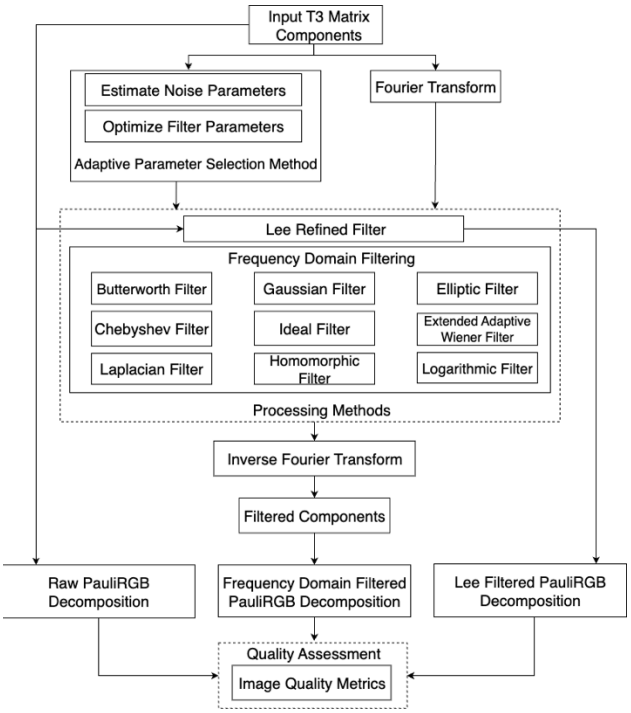

Fig. 1. Schematic representation of the proposed PolSAR image filtering and evaluation methodology

To optimize filter performance across different T3 matrix elements, a dynamic parameter selection approach was implemented. This approach begins with a comprehensive noise parameter estimation for each T3 component, followed by adaptive parameter tuning for each filter type. The dynamic parameter selection enhances the filtering process by adjusting parameters based on the specific characteristics of each T3 matrix element, resulting in improved speckle reduction while preserving important structural information.

The noise parameter estimation process encompasses several key metrics. First, the ENL is calculated for homogeneous regions to provide an initial assessment of speckle intensity. SNR measurements offer insights into the relative strength of the signal compared to the noise. The estimated noise variance is computed using robust statistical methods to account for the multiplicative nature of speckle in SAR imagery. Local variance values are calculated within sliding windows across the image to capture spatial variations in noise distribution. Additionally, global mean values and standard deviations are computed for each T3 matrix element to establish baseline statistical properties (Shanmugavadivu and Shanthasheela, 2014).

Based on these estimated noise parameters, filter-specific parameters are dynamically optimized for each T3 matrix element. Window size adaptation adjusts the spatial extent of filtering operations according to the local statistical properties, with larger windows applied to homogeneous regions and smaller windows preserved for areas with fine details. Sigma value adaptation for Gaussian and related filters is performed by scaling the standard deviation parameter based on the estimated noise level and local variance. Cutoff frequency parameters for filters such as Butterworth, Chebyshev, Elliptic, and Ideal are adjusted according to the frequency characteristics observed in the power spectrum of each T3 component. Furthermore, filter-specific parameters such as order values for Butterworth and Chebyshev filters, ripple specifications for Elliptic filters, and scaling factors for Homomorphic and Logarithmic filters are fine-tuned based on the unique properties of each matrix element.

The quality of both original and filtered images is assessed using five different image quality metrics. The equations of the image quality metrics are adopted from (Mittal, Moorthy, and Bovik, 2012; Sara, Akter, and Uddin, 2019).

3.1 SSIM Score

It compares structural similarity between filtered images and the original image, considering luminance, contrast, and structure components. It ranges from 0 to 1, where higher SSIM values mean better preservation of structural details. The mathematical formulation of the SSIM score is given by eq. (4), where μ_X and μ_Y are the mean values σ_X^2 and σ_Y^2 are the variances, and C_1, C_2 are constants.

$$\mathrm{SSIM}(X,Y) = \frac{(2\mu_X\mu_Y+C_1)(2\sigma_{XY}+C_2)}{(\mu_X^2+\mu_Y^2+C_1)(\sigma_X^2+\sigma_Y^2+C_2)} \quad (4)$$

3.2 PSNR Score

It quantifies the ratio between the maximum possible signal strength and the noise introduced by filtering, typically measured in decibels (dB). Higher PSNR values indicate better preservation of the original image with minimal noise. The mathematical formulation of the PSNR score is given by eq. (5), where MAX is the maximum possible pixel value (e.g., 255 for an 8-bit image).

$$\mathrm{PSNR} = 10\log_{10}\left(\frac{\mathrm{MAX}^2}{\mathrm{MSE}}\right) \quad (5)$$

3.3 CV Score

It measures the relative variability in intensity in a single patterned area, helping to judge noise in textured segments. A lower CV indicates less noise and better consistency in the image. CV is the ratio of standard deviation over mean intensity. The mathematical formulation of the CV score is given by eq. (6), where σ is variance and μ is mean value.

$$\mathrm{CV} = \frac{s}{\mu} \quad (6)$$

3.4 ENL Score

It quantifies the smoothness of these images by estimating the effective averaging of independent noise samples. A higher ENL value indicates reduced speckle noise and better homogeneity within the image. ENL is computed as the squared ratio of the average intensity to its standard deviation in a homogenous region. The mathematical formulation of the ENL score is given by eq. (7), where σ is variance and μ is mean value.

$$\mathrm{ENL} = \left(\frac{\mu}{\sigma}\right)^2 \quad (7)$$

3.5 SNR Score

It evaluates the ratio of signal strength to noise magnitude. Higher SNR values reflect cleaner images with minimal noise corruption. SNR can be expressed in linear form as the ratio of the mean signal intensity to the standard deviation of noise, or in decibels, which involves a logarithmic transformation of this ratio. The mathematical formulation of the SNR score is given by eq. (8), where σ is variance and μ is mean value.

$$\mathrm{SNR} = 20\log_{10}\left(\frac{\mu}{\sigma}\right) \quad (8)$$

This evaluation enables a comparative analysis of filter performance across T3 matrix elements, with the Lee Refined filter serving as a benchmark due to its widely recognized effectiveness (Lee et al., 1999,). The performance characteristics of frequency domain filters applied to T3 matrix components across different image quality metrics are quantitatively evaluated as shown in Figure 2. The comparative analysis reveals filter-specific strengths in processing different T3 matrix elements, with certain filters showing superior performance for specific elements while exhibiting limitations for others.

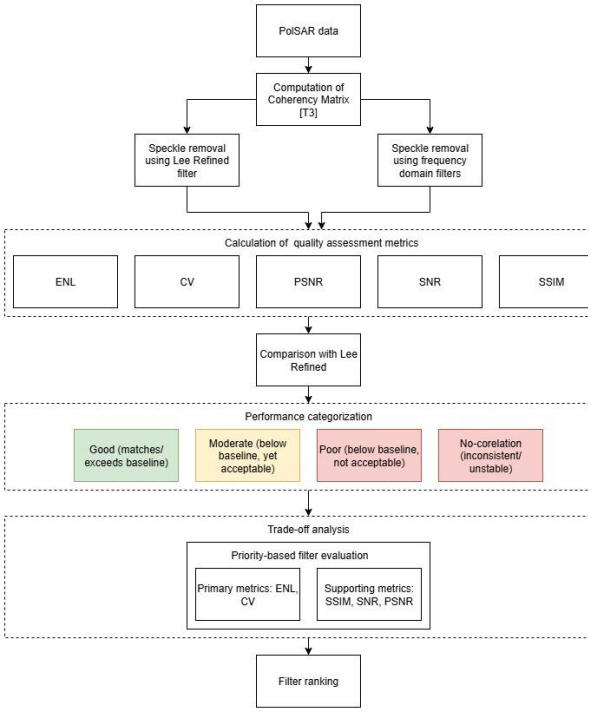

Fig. 2. Methodology flowchart for comparative evaluation of frequency domain filters across T3 matrix components

4. RESULTS AND DISCUSSION

4.1 Equivalent Number of Looks (ENL): Speckle Reduction Effectiveness

The ENL analysis reveals the speckle reduction capabilities of different filters in homogeneous regions compared to the Lee Refined filter baseline (0.359-2.526 across T3 components), based on results obtained as shown in Fig. 3. Higher ENL indicates smoother, less noisy image regions. Table 1 further summarizes the ENL performance of each filter.

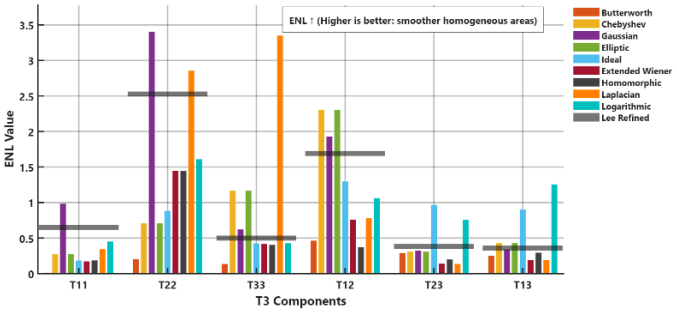

Fig. 3. ENL comparison of T3 components across different frequency domain filters

Table 1. Equivalent Number of Looks (ENL) Performance

Filter	ENL Range	Performance Category	Comparison to Lee Refined Filter
Lee Refined (Baseline)	0.359-2.526	Reference	-
Gaussian	Up to 3.4	Good	Substantially exceeds baseline
Laplacian	Up to 3.3	Good	Substantially exceeds baseline
Chebyshev	0.4-2.3	Good	Matches/slightly below baseline
Elliptic	0.3-2.3	Good	Variable around baseline
Homomorphic	Below 1.0	Moderate	Below baseline
Logarithmic	0.2-1.6	Moderate	Mostly below baseline
Extended Adaptive Wiener	0.2-1.5	Moderate	Below baseline
Ideal	Below 1.0	Moderate	Significantly below baseline
Butterworth	0.1-0.5	Poor	Significantly below baseline

4.1.1. Good Performance

The Gaussian filter achieved the highest ENL values across all evaluated filters, reaching up to 3.4 for the T22 component of the coherency matrix, significantly exceeding the Lee Refined filter's maximum of 2.526. This can be attributed to the Gaussian filter's uniform smoothing effect, which effectively reduces local variance in homogeneous regions without explicitly preserving edge information (Argenti *et al.*, 2012).

The Laplacian filter also yielded high ENL values, reaching up to 3.3, surpassing the Lee Refined filter in terms of noise reduction in flat regions. This performance is due to its second-order derivative response, which attenuates intensity variations in homogeneous areas, resulting in reduced variance and elevated ENL (Podder *et al.*, 2014).

The Chebyshev filter showed moderate ENL performance, with values ranging from 0.4 to 2.3, generally matching or slightly underperforming the Lee Refined baseline. This is likely due to its sharp cutoff characteristics, which may introduce passband ripples that reduce consistency in noise suppression (Ives *et al.*, 2003).

The Elliptic filter exhibited variable performance (ENL: 0.3-2.3), with the T3 components demonstrating comparable speckle reduction to the Lee Refined filter. Its steep transition band and equi-ripple behavior enable selective filtering, though

they may also cause uneven smoothing, leading to variation in ENL across components (Ives *et al.*, 2003).

4.1.2. Moderate Performance

The Homomorphic filter exhibited limited ENL performance, with values below 1.0 for most components (T11, T33, T12, T13, T23) and remained below the baseline established by the Lee Refined filter. This outcome may be related to the application of logarithmic transformation followed by high-pass filtering, which tends to retain high-frequency content such as speckle, thereby reducing the effectiveness of variance suppression in homogeneous regions (Hoekman *et al.*, 2011).

The Logarithmic filter yielded ENL values in the range of 0.2 to 1.6, generally lower than those observed with the Lee Refined filter. The nonlinear transformation applied in this method modifies both signal and noise levels, which may result in variation in speckle reduction performance across different components (Hoekman *et al.*, 2011).

The Extended Adaptive Wiener filter produced ENL values between 0.2 and 1.5, indicating a lower degree of speckle suppression compared to the Lee Refined filter. This may be due to its reliance on local statistical properties to guide filtering, which may limit the extent of smoothing in uniform image regions (Singh *et al.*, 2013).

The Ideal filter showed minimal improvement in ENL, with values typically remaining below 1.0. The sharp frequency cutoff characteristic of this filter may not adequately reduce noise components, leading to reduced effectiveness in homogeneous regions when compared with the Lee Refined filter (Bourennane *et al.*, 2007).

4.1.3. Poor Performance

The Butterworth filter showed consistently low ENL values (0.1-0.5), indicating poor speckle reduction capabilities significantly below the Lee Refined performance. This may be attributed to its smooth frequency roll-off, which provides limited separation between signal and noise components, thereby reducing its effectiveness in attenuating high-frequency speckle noise in homogeneous regions (Ives *et al.*, 2003).

4.2 Coefficient of Variation (CV): Intensity Distribution Uniformity

The CV analysis examines the filters' ability to maintain uniform intensity distributions compared to the Lee Refined baseline (0.603-1.398 across T3 components), based on results obtained as shown in Fig. 4. A lower CV value indicates better speckle suppression and higher uniformity in homogeneous regions. Table 2 further summarizes the CV performance of each filter.

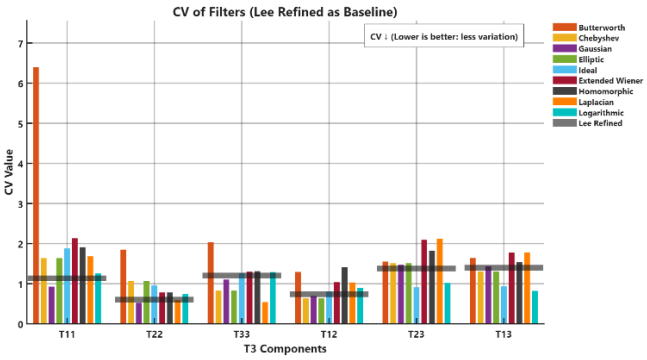

Fig. 4. CV comparison of T3 components across different frequency domain filters

Table 2. Coefficient of Variation (CV) Performance

Filter	CV Range	Performance Category	Comparison to Lee Refined Filter
Lee Refined (Baseline)	0.603-1.398	Reference	-
Gaussian	0.5-1.5	Good	Competes with baseline
Chebyshev	0.7-1.6	Good	Comparable to baseline
Logarithmic	0.8-1.5	Good	Competes with baseline
Elliptic	0.8-1.8	Good	Within baseline range
Extended Adaptive Wiener	0.8-2.2	Moderate	Comparable to baseline
Homomorphic	0.8-2.0	Moderate	Matches baseline
Laplacian	0.8-2.1	Moderate	Variable around baseline
Ideal	0.9-2.0	Moderate	Variable around baseline
Butterworth	1.0-2.0 (spike to 6.4)	No correlation	Inconsistent performance

4.2.1. Good Performance

The Gaussian filter demonstrated uniform intensity distributions with low CV values (0.5-1.5), indicating stable behaviour comparable to the Lee Refined performance. This outcome can be attributed to its symmetric low-pass characteristics, which effectively reduce local variance while maintaining the mean in homogeneous areas (Argenti *et al.*, 2012).

The Chebyshev filter showed similar performance, maintaining low CV values (0.7-1.6) comparable to the Lee Refined baseline. Its steeper roll-off helps in attenuating high-frequency variations, contributing to improved uniformity while preserving signal characteristics in flat regions (Ives *et al.*, 2003).

The Logarithmic filter maintained CV values in the range of 0.8-1.5, suggesting stable output. This behaviour may result from the logarithmic transformation's ability to compress dynamic range, which helps to balance intensity fluctuations.

The Elliptic filter exhibited good CV performance, with values ranging from 0.8-1.8, mostly within the Lee Refined range. Its sharp transition band allows for selective attenuation of undesired frequency components, supporting uniformity in areas of low structural variation (Ives *et al.*, 2003).

4.2.2. Moderate Performance

The Extended Adaptive Wiener filter demonstrated moderate performance (CV: 0.8-2.2) with uniformity levels comparable to the Lee Refined baseline. This behaviour may result from its adaptive design, which adjusts filtering based on local variance, providing smoothing that varies with regional image statistics.

The Homomorphic filter demonstrated uniformity with CV values ranging from 0.8-2.0, aligning with the Lee Refined performance. This can be attributed to the logarithmic transformation reducing the impact of multiplicative noise,

which supports improved intensity balance in low-variance regions (Hoekman *et al.*, 2011).

The Laplacian filter showed variable performance with CV values between 0.8-2.1, reflecting component-specific outcomes around the Lee Refined baseline. This may be due to its derivative-based operation, which enhances intensity transitions and can increase local variance in some areas.

The Ideal filter displayed moderate CV values (0.9-2.0), which, combined with its lower performance in other metrics, indicates limited ability to suppress local variations. Its sharp frequency cutoff may reduce effectiveness in noise attenuation near the cutoff region, affecting intensity uniformity (Bourennane *et al.*, 2007).

4.2.3. No-correlation/Poor Performance

The Butterworth filter showed variable CV performance ranging from 1.0-2.0, with one notable spike to approximately 6.4 for T11 component. This variation, together with its low ENL values, indicates limited effectiveness in achieving uniform intensity distributions and suggests that the filter's speckle suppression capability varies significantly across image regions (Ives *et al.*, 2003).

4.3 Peak Signal-to-Noise Ratio (PSNR): Image Fidelity Preservation

The PSNR analysis demonstrates image fidelity preservation capabilities, with detailed comparison against the Lee Refined filter baseline which shows component-specific performance ranging from 33.5 dB (T33) to 47.1 dB (T11), with notable variations across different T3 matrix elements. The analysis is based on results obtained as shown in Fig. 5. Table 3 further summarizes the PSNR performance of each filter.

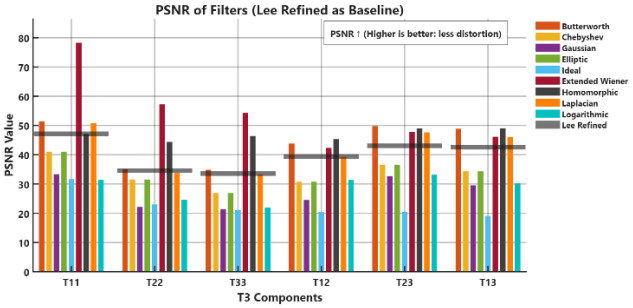

Fig. 5. PSNR comparison of T3 components across different frequency domain filters

Table 3. Peak Signal-to-Noise Ratio (PSNR) Performance

Filter	PSNR Range	Performance Category	Comparison to Lee Refined Filter
Lee Refined (Baseline)	33.5-47.1	Reference	-
Extended Adaptive Wiener	Upto 78	Good	Substantially exceeds baseline
Homomorphic	45-52	Good	Matches/exceeds baseline
Laplacian	40-52	Moderate	Generally surpasses baseline
Butterworth	35-51	Moderate	Mixed performance
Chebyshev	27-41	Moderate	Generally below baseline
Elliptic	25-42	Moderate	Mixed performance
Gaussian	21-35	Poor	Below baseline
Logarithmic	21-35	Poor	Below baseline
Ideal	20-32	Poor	Significantly below baseline

4.3.1. Good Performance

The Extended Adaptive Wiener filter demonstrated the highest PSNR performance, reaching up to 78 dB for T11 component of the coherency matrix, substantially exceeding the Lee Refined filter's peak performance of 47.1 dB. This indicates effective preservation of original image information with minimal distortion, likely due to its adaptive approach that balances noise reduction with detail retention.

The Homomorphic filter showed competitive PSNR performance with values ranging from 45-52 dB, consistently matching or exceeding the Lee Refined baseline. This may be attributed to its logarithmic transformation, which compresses dynamic range and enhances signal fidelity by reducing multiplicative noise effects (Hoekman *et al.*, 2011).

The Laplacian filter demonstrated strong performance with PSNR values between 40-52 dB, generally surpassing the Lee Refined filter's component-specific levels. Its second-order derivative operation sharpens edges while smoothing homogeneous regions, aiding in preserving image structure and improving fidelity.

The Butterworth filter exhibited good PSNR performance ranging from 35-51 dB, with T3 components either matching or exceeding the Lee Refined baseline. Its smooth frequency response provides balanced noise attenuation without excessive blurring, supporting effective signal preservation (Ives *et al.*, 2003).

4.3.2. Moderate Performance

The Chebyshev filter showed moderate PSNR values (27-41 dB) with component-specific variations that generally underperform the Lee Refined baseline. This may be due to its equiripple nature, which can introduce passband distortions affecting overall signal fidelity. The Elliptic filter exhibited moderate PSNR values (25-42 dB), with mixed performance relative to the Lee Refined baseline, possibly reflecting its steep transition bands that may cause ripples and uneven noise suppression (Ives *et al.*, 2003).

4.3.3. Poor Performance

The Logarithmic and Gaussian filters exhibited lower PSNR values, typically ranging from 21-35 dB, ie. below the Lee Refined baseline. The Logarithmic filter's nonlinear transformation can amplify noise components, while the Gaussian filter's smoothing may overly blur fine details, both contributing to reduced fidelity (Argenti *et al.*, 2012). The Ideal filter demonstrated the lowest PSNR values (20-32 dB) across all T3 components, in line with its poor performance in other metrics. Its abrupt frequency cutoff tends to introduce ringing artifacts and insufficient noise attenuation, leading to diminished image quality (Bourennane *et al.*, 2007).

4.4 Signal-to-Noise Ratio (SNR): Quality Enhancement Assessment

The SNR analysis reveals complex performance patterns across different filtering approaches compared to the Lee Refined

baseline (4.818-11.424 dB across T3 components), based on results obtained as shown in Fig. 6. Table 4 further summarizes the SNR performance of each filter.

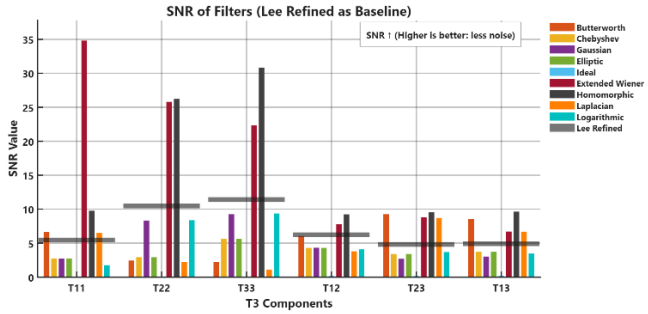

Fig. 6. SNR comparison of T3 components across different frequency domain filters

Table 4. Signal-to-Noise Ratio (SNR) Performance

Filter	SNR Range	Performance Category	Comparison to Lee Refined Filter
Lee Refined (Baseline)	4.818-11.424	Reference	-
Extended Adaptive Wiener	Up to 35	Good	Substantially exceeds baseline
Homomorphic	8-25	Good	Often exceeds baseline
Logarithmic	2-10	Moderate	Occasionally matches baseline
Gaussian	2-9	Moderate	Generally below baseline
Laplacian	2-9	Moderate	Generally below baseline
Butterworth	3-9	Moderate	Below baseline
Chebyshev	3-6	Moderate	Below baseline
Elliptic	3-6	Moderate	Below baseline
Ideal	Below 0.2	Poor	Significantly below baseline

4.4.1. Good Performance

The Extended Adaptive Wiener filter demonstrated notable SNR improvement, reaching up to 35 dB for T11 component of the coherency matrix, likely due to its adaptive smoothing which balances noise suppression with preservation of structural details. The Homomorphic filter showed consistent SNR performance ranging from 8-25 dB, often exceeding the Lee Refined baseline, which may be attributed to its logarithmic processing reducing multiplicative noise effects (Hoekman *et al.*, 2011).

4.4.2. Moderate Performance

The Logarithmic filter showed variable but strong SNR performance (2-10 dB), occasionally matching the Lee Refined range, potentially due to its nonlinear contrast enhancement affecting signal and noise differently. The Gaussian and Laplacian filters exhibited moderate SNR values (2-9 dB), generally below the Lee Refined peak, as their smoothing and derivative operations may blur fine details or amplify noise components. Traditional frequency domain filters such as Butterworth, Chebyshev, and Elliptic showed consistently lower SNR values; Butterworth ranged from 3-9 dB, while Chebyshev and Elliptic filters had narrower windows of 3-6 dB. These lower values reflect limitations in balancing noise reduction and detail preservation across all components (Ives *et al.*, 2003).

4.4.3. Poor Performance

The Ideal filter showed minimal SNR values, often below 0.2 dB, significantly below the Lee Refined filter. This is likely due to its abrupt frequency cutoff causing ringing artifacts and ineffective noise attenuation, which severely impacts signal reconstruction quality (Bourennane *et al.*, 2007).

4.5 Structural Similarity Index Measure (SSIM): Assessing Structural Preservation

The SSIM analysis reveals critical insights into how different filtering approaches preserve structural information compared to the Lee Refined filter baseline based on results obtained as shown in Fig. 7. Table 5 further summarizes the SSIM performance of each filter.

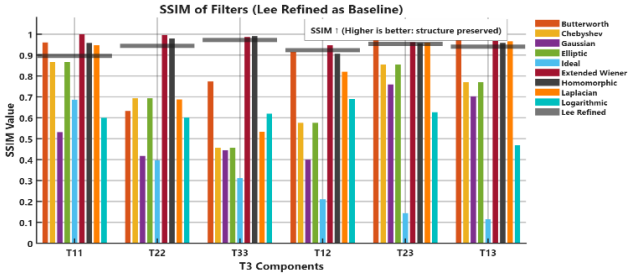

Fig. 7. SSIM comparison of T3 components across different frequency domain filters

Table 5. Structural Similarity Index Measure (SSIM) Performance

Filter	SSIM Range	Performance Category	Comparison to Lee Refined Filter
Lee Refined (Baseline)	0.896 - 0.972	Reference	-
Extended Adaptive Wiener	0.95-1.0	Good	Often matches/exceeds baseline
Homomorphic	0.90-0.98	Good	Often surpasses baseline
Laplacian	0.55-0.95	Moderate	Mixed performance
Butterworth	0.65-0.98	Moderate	Mixed performance
Chebyshev	0.45-0.85	Moderate	Generally below baseline
Elliptic	0.40-0.85	Moderate	Generally below baseline
Gaussian	0.45-0.80	Moderate	Below baseline
Logarithmic	0.50-0.75	Moderate	Below baseline
Ideal	0.12-0.30	Poor	Significantly below baseline

4.5.1. Good Performance

The Extended Adaptive Wiener filter showed SSIM values between 0.95-1.0, often matching or slightly exceeding the Lee Refined performance (0.896-0.972). This is attributed to its adaptive smoothing approach, which balances noise suppression with the preservation of structural details. The Homomorphic filter demonstrated SSIM values ranging from 0.90-0.98 across all components, reflecting its use of

logarithmic transformation that reduces multiplicative noise effects while maintaining structural information across polarimetric channels (Hoekman *et al.*, 2011).

4.5.2. Moderate Performance

The Laplacian filter exhibited a wide range of SSIM values (0.55-0.95), indicating variability in structural similarity among components. Its second-order derivative operation enhances edges but can amplify noise in some regions, leading to variable similarity relative to the Lee Refined baseline. The Elliptic filter presented SSIM values between 0.40 and 0.85, with component-specific differences likely caused by steep transition bands introducing passband ripples that affect structural preservation. Butterworth and Chebyshev filters showed mixed results; Butterworth's SSIM ranged from 0.65 to 0.98, indicating varying levels of structural preservation across components, while Chebyshev ranged from 0.45 to 0.85, reflecting component-dependent performance potentially influenced by ripple effects in the filter response (Ives *et al.*, 2003). The Gaussian filter had moderate SSIM values (0.40-0.80), generally lower than the Lee Refined baseline, possibly due to uniform smoothing that reduces noise but may also diminish fine structural details. The Logarithmic filter exhibited SSIM values between 0.50 and 0.70, generally below the Lee Refined baseline, which may result from nonlinear contrast enhancement affecting structural consistency.

4.5.3. Poor Performance

The Ideal filter showed the lowest SSIM values (0.12–0.70) across components. Its abrupt frequency cutoff is likely responsible for ringing artifacts and loss of structural information, contributing to reduced image quality compared to the Lee Refined filter (Bourennane *et al.*, 2007).

4.6 Comparative Analysis and Performance Trade-offs

Table 6. Summary of Filter Performance Across All Metrics

Filter	CV	SNR	ENL	SSIM	PSNR
Lee Refined	1.074	7.219	1.016	0.933	42.672
Butterworth	2.368	6.462	0.268	0.923	45.438
Chebyshev	1.089	4.018	**1.130**	0.683	33.381
Gaussian	1.052	4.392	1.020	0.540	27.673
Elliptic	1.089	4.018	**1.130**	0.683	33.381
Ideal	1.096	0.133	0.844	0.279	22.160
Extended Wiener	1.263	**14.708**	0.806	**0.967**	**51.870**
Homomorphic	1.568	13.046	0.304	0.946	47.046
Laplacian	1.363	5.102	0.930	0.840	42.726
Logarithmic	**1.026**	4.412	0.835	0.615	29.931

Table 6 presents averaged values across all T3 matrix components. The metrics collectively assess each filter's ability to suppress speckle noise while preserving image structure and texture. Lower CV values indicate better speckle suppression consistency, while higher SNR and PSNR reflect stronger noise reduction capabilities. SSIM evaluates structural fidelity, and ENL indicates the preservation of homogeneous regions.

The results indicate that the Extended Adaptive Wiener filter attains the highest SNR (14.708) and PSNR (51.870) among the evaluated filters. It also maintains a SSIM (0.967), marginally exceeding that of Lee Refined (0.933), which suggests effective structural preservation. Although its CV (1.263) is moderately higher than Lee Refined (1.074), indicating potential over smoothing, and its ENL (0.806) is lower, suggesting less effective smoothing in homogeneous regions, these factors are balanced by its substantial noise suppression and maintenance of structural details.

Other filters such as Logarithmic, Chebyshev, and Elliptic present lower CV values (approximately 1.026 to 1.089) and higher ENL values (approximately 0.835 to 1.130) compared to Extended Wiener, reflecting more consistent speckle suppression and better smoothing in uniform areas. However, their lower SNR, SSIM, and PSNR values indicate reduced effectiveness in noise reduction and structural clarity, which are critical for SAR image analysis.

Conversely, Butterworth and Homomorphic filters provide increased PSNR values but exhibit substantially higher CV and lower ENL, implying increased over smoothing and diminished texture preservation.

4.6.1. Key Findings

The analysis identifies the Equivalent Number of Looks (ENL) as a key metric for assessing speckle suppression effectiveness in homogeneous regions of the image. The Lee Refined filter demonstrates an ENL of 1.016, indicating a balanced approach that moderately reduces speckle while preserving image details. Chebyshev and Elliptic filters exhibit slightly higher ENL values (~1.130), suggesting marginally increased smoothing in uniform areas. Gaussian filtering closely aligns with Lee Refined in ENL (1.020) but presents lower structural similarity (SSIM), indicating some compromise in image structure preservation. The Extended Adaptive Wiener filter shows a moderate ENL of 0.806, reflecting a reasonable level of speckle reduction, while the Homomorphic filter's ENL of 0.304 points to less effective smoothing in homogeneous regions. The Butterworth filter records the lowest ENL at 0.268, which may indicate either noise retention or over-sharpening effects in flat areas.

Coefficient of Variation (CV) is considered an indicator of intensity uniformity, with lower values representing more consistent pixel intensities. Gaussian (1.052) and Logarithmic (1.026) filters demonstrate CV values comparable to Lee Refined (1.074). Chebyshev and Elliptic filters also maintain CV values close to this baseline, suggesting stable intensity distribution in homogeneous regions. Extended Wiener presents a CV of 1.263, which may indicate a balance between smoothing and texture retention. Homomorphic filtering has a higher CV of 1.568, which could reflect increased smoothing or texture loss. The Butterworth filter's CV of 2.368 suggests greater intensity variation and less uniform filtering outcomes.

Additional metrics such as Signal-to-Noise Ratio (SNR), Structural Similarity Index (SSIM), and Peak Signal-to-Noise Ratio (PSNR) provide important perspectives on filter performance. Extended Wiener records the highest SNR (14.708) and PSNR (51.870), accompanied by a high SSIM of 0.967, indicating effective noise suppression with strong structural similarity. Homomorphic filtering achieves elevated SNR (13.046) and PSNR (47.046) values with an SSIM of 0.946, suggesting good noise suppression while retaining structural features. Butterworth shows a slightly lower SSIM (0.923) despite reasonable PSNR (45.438), indicating compromise in structural fidelity. Laplacian filtering presents a moderate SSIM of 0.840, reflecting a trade-off between texture preservation and noise reduction. Chebyshev and Elliptic filters exhibit lower SSIM values near 0.683, which corresponds with reduced structural similarity. Gaussian and Logarithmic filters have SSIM values of 0.540 and 0.615 respectively, suggesting diminished preservation of image structure. The Ideal filter

shows the lowest SSIM (0.279), alongside minimal SNR and PSNR, indicative of limited effectiveness in noise reduction and structural maintenance.

4.6.2. Performance Trade-offs

The trade-offs observed indicate that Extended Wiener offers the best denoising performance, but at the cost of moderate texture preservation (CV and ENL). Conversely, Lee Refined achieves a good compromise between structure and texture, making it ideal for balanced applications. Filters like Butterworth and Homomorphic are strong in SNR and PSNR, but their poor ENL and CV values indicate a significant loss in homogeneous region quality, which is critical in SAR imagery.

Other frequency-domain filters like Chebyshev, Elliptic, and Gaussian maintain strong ENL and CV performance but suffer in SSIM and PSNR, indicating that while they may smooth flat regions, they fail to preserve structural features and edges, making them less suitable for de-speckling applications. The Ideal filter, despite its sharp frequency cutoff, shows drastically poor results across all metrics, highlighting its incompatibility with speckle reduction tasks in SAR images.

Overall, despite the tradeoffs in CV and ENL, Extended Adaptive Wiener filter remains the most effective choice, as its superior noise suppression (highest SNR and PSNR) combined with excellent structural preservation (highest SSIM) makes it the best performing frequency domain filter for SAR de-speckling applications, especially where noise reduction and structural clarity are critical.

4.7 Conclusion

This study analyses the effectiveness of frequency domain filtering techniques in the de-speckling of SAR imagery. Compared to traditional spatial domain methods, frequency-based filters offer greater flexibility in targeting noise components while preserving essential image structures. Their ability to operate in the spectral domain enables better separation of signal from noise, making them highly suitable for advanced remote sensing applications such as object recognition, land cover classification, and image compression, where structural and textural fidelity is critical.

Frequency domain filtering enables precise separation of speckle noise and image detail by operating on the Fourier spectrum, ensuring targeted noise removal without sacrificing edges or textures. It also primes the data for advanced multiscale transforms such as wavelet and curvelet filtering. Its compatibility with FFTs makes it computationally efficient for large SAR datasets, and its ability to preserve spectral signatures enhances downstream tasks like classification, object detection, and compression. Therefore, frequency-domain filters offer both performance and efficiency advantages that are essential for high-quality SAR image analysis.

Among the filters analysed, the Extended Adaptive Wiener filter consistently delivers strong performance, achieving the highest SNR, PSNR, and SSIM values across multiple test scenarios. It proves highly effective at suppressing speckle noise while retaining structural integrity. Although it shows a slightly lower ENL compared to the Lee Refined filter, this trade-off is often acceptable, especially in applications that prioritize edge clarity and feature preservation over uniformity in flat regions.

Importantly, the Extended Adaptive Wiener filter offers performance comparable to the Lee Refined filter, which has long been established as a baseline for spatial domain de-speckling. The Extended Adaptive Wiener filter even surpasses Lee Refined in denoising metrics like SNR, PSNR and SSIM. This makes it not only a viable alternative but also a preferable choice in frequency-sensitive or high-precision image processing workflows.

In conclusion, the Extended Adaptive Wiener filter stands out as a powerful, reliable, and efficient solution for SAR de-speckling in the frequency domain. It bridges the gap between effective noise suppression and structure preservation, offering performance that is on par with, and in many cases better to the widely used Lee Refined filter. Its application potential extends beyond de-speckling, positioning it as a valuable tool in a wide range of remote sensing and image analysis tasks, from classification and object detection to compression and real-time enhancement. With further optimization and integration into learning-based systems, frequency domain filters like Extended Adaptive Wiener filter are poised to play a pivotal role in the future of Earth observation technologies.

Looking ahead, hybrid approaches that combine Extended Adaptive Wiener filter with complementary spatial-domain or machine-learning-based methods offer a promising avenue. By fusing the strengths of frequency-domain denoising and contextual adaptation, such hybrids could further enhance de-speckling performance, robustness, and computational efficiency. Integrating Extended Adaptive Wiener filter into hybrid or deep-learning frameworks will be key to unlocking next-generation Earth-observation tools, from high-fidelity terrain classification and object detection to real-time image enhancement and compression.

5. REFERENCES

[1] A. Achim, E. E. Kuruoglu, and J. Zerubia, "SAR Image Filtering Based on the Heavy-Tailed Rayleigh Model," *Research Report RR-5493, INRIA*, 2006, pp. 1–21. doi: 10.1109/TIP.2006.877362

[2] A. Alam and A. Rai, “Reduction of speckle noise in SAR images with hybrid wavelet filter,” *Int. J. Res. Appl. Sci. Eng. Technol. (IJRASET)*, vol. 10, no. 7, Jul. 2022. doi: 10.22214/ijraset.2022.46014

[3] A. Masurkar, R. Daruwala, and V. Turkar, "A novel method to remove speckle from POLSAR images using morphological operations," in *Proc. IEEE Int. Geoscience and Remote Sensing Symp. (IGARSS)*, 2020, pp. 126–129. doi: 10.1109/IGARSS39084.2020.9321234

[4] A. Mittal, A. K. Moorthy, and A. C. Bovik, “No-reference image quality assessment in the spatial domain,” *IEEE Trans. Image Process.*, vol. 21, no. 12, pp. 4695–4708, Dec. 2012. doi: 10.1109/TIP.2012.2214050

[5] B. Kanoun, G. Ferraioli, V. Pascazio, and G. Schirinzi, "Fast GPU-Based Enhanced Wiener Filter for Despeckling SAR Data," *Remote Sensing*, vol. 11, no. 12, p. 1473, Jun. 2019. doi: 10.3390/rs11121473

[6] C. Ju and C. R. Moloney, “An edge-enhanced modified Lee filter for the smoothing of SAR image speckle noise,” in *Proc. IEEE Int. Geoscience and Remote Sensing Symp. (IGARSS)*, 1998.

[7] C. Oliver and S. Quegan, *Understanding Synthetic Aperture Radar Images*, SciTech Publishing, 2004. ISBN: 978-1891121319.

[8] D. H. Hoekman, M. A. M. Vissers, and T. N. Tran, "Unsupervised Full-Polarimetric SAR Data Segmentation as a Tool for Classification of Agricultural Areas," *IEEE*

J. Sel. Topics Appl. Earth Observ. Remote Sens., vol. 4, no. 2, pp. 402–411, Jun. 2011. doi: 10.1109/JSTARS.2010.2042280

[9] D. Hazarika, V. K. Nath, and M. Bhuyan, "SAR Image Despeckling Based on Combination of Laplace Mixture Distribution with Local Parameters and Multiscale Edge Detection in Lapped Transform Domain," *Procedia Comput. Sci.*, vol. 87, 2016. doi: 10.1016/j.procs.2016.05.140

[10] F. Argenti, A. Lapini, T. Bianchi, and L. Alparone, "A tutorial on speckle reduction in synthetic aperture radar images," *IEEE Geosci. Remote Sens. Mag.*, vol. 1, no. 3, pp. 6–35, 2013. doi: 10.1109/MGRS.2013.2282038

[11] F. Argenti, T. Bianchi, A. Lapini, and L. Alparone, "Fast MAP despeckling based on Laplacian–Gaussian modeling of wavelet coefficients," *IEEE Geosci. Remote Sens. Lett.*, vol. 9, no. 1, pp. 13–17, Jan. 2012. doi: 10.1109/LGRS.2011.2158798

[12] F. Del Frate, G. Schiavon, D. Solimini, M. Borgeaud, D. H. Hoekman, and M. A. M. Vissers, "Crop classification using multiconfiguration C-band SAR data," *IEEE Trans. Geosci. Remote Sens.*, vol. 41, no. 7, pp. 1611–1619, Jul. 2003. doi: 10.1109/TGRS.2003.813530

[13] H. Salehi, J. Vahidi, T. Abdeljawad, A. Khan, and S. Y. B. Rad, "A SAR Image Despeckling Method Based on an Extended Adaptive Wiener Filter and Extended Guided Filter," *Remote Sensing*, vol. 12, no. 15, p. 2371, Jul. 2020. doi: 10.3390/rs12152371

[14] J.-S. Lee, "Refined filtering of image noise using local statistics," *Comput. Graph. Image Process.*, vol. 15, no. 4, pp. 380–389, 1981. doi: 10.1016/S0146-664X(81)80018-4

[15] J.-S. Lee, L. Jurkevich, P. Dewaele, P. Wambacq, and A. Oosterlinck, "Speckle filtering of synthetic aperture radar images: A review," *Remote Sensing Reviews*, vol. 8, 1994. doi: 10.1080/02757259409532206

[16] J.-S. Lee, M. R. Grunes, and G. de Grandi, "Polarimetric SAR speckle filtering and its implication for classification," *IEEE Trans. Geosci. Remote Sens.*, vol. 37, no. 5, pp. 2363–2373, 1999. doi: 10.1109/36.789635

[17] J. A. Richards, *Remote Sensing Digital Image Analysis: An Introduction*, 4th ed., New York, NY, USA: Springer, 2013. ISBN: 978-1461480816.

[18] J. Ansari, S. M. Ghosh, M. Dev Behera, and S. Kumar Gupta, "A Study on Speckle Removal Techniques for Sentinel-1A SAR Data Over Sundarbans, Mangrove Forest, India," in *Proc. IEEE India Geosci. Remote Sens. Symp. (InGARSS)*, 2020, pp. 90–93. doi: 10.1109/InGARSS48198.2020.9358929

[19] J. L. Zhu, J. Wen, and Y. Zhang, "A new algorithm for SAR image despeckling using an enhanced Lee filter and median filter," in *Proc. 6th Int. Congr. Image and Signal Processing (CISP)*, vol. 1, pp. 224–228, 2013. doi: 10.1109/CISP.2013.6743991

[20] P. Podder, M. M. Hasan, M. R. Islam, and M. Sayeed, "Design and implementation of Butterworth, Chebyshev-I and Elliptic filter for speech signal analysis," *Int. J. Comput. Appl.*, vol. 98, no. 7, pp. 12–18, Jul. 2014. doi: 10.5120/17195-7390

[21] P. S. Tondewad and M. P. Dale, "Denoising of SAR Images using Wavelet Transforms and Wiener Filter," in *Proc. Int. Conf. Emerging Smart Comput. Informatics (ESCI)*, Pune, India, 2023, pp. 1–5. doi: 10.1109/ESCI56872.2023.10100330

[22] P. Shanmugavadivu and A. Shanthasheela, "Feature Variance Based Filter For Speckle Noise Removal," *IOSR J. Comput. Eng. (IOSR JCE)*, vol. 16, no. 5, ver. I, pp. 15–19, Sep.–Oct. 2014. doi: 10.9790/0661 16511519

[23] R. R. Mohan, S. Mridula, and P. Mohanan, "Speckle noise reduction in images using Wiener filtering and adaptive Wavelet thresholding," in *Proc. IEEE Region 10 Conf. (TENCON)*, 2016, pp. 2860–2863. doi: 10.1109/TENCON.2016.7848566

[24] R. W. Ives, D. M. Etter, and T. B. Welch, "Speckle reduction of SAR imagery using homomorphic processing and predictive filtering," in *Proc. Asilomar Conf. Signals, Syst. Comput.*, Pacific Grove, CA, USA, Nov. 2003, pp. 216–220. doi: 10.1109/ACSSC.2003.1291901

[25] S. A. G., D. P. Vasuki, and A. A. Deepan, "Hybrid Laplacian Gaussian Based Speckle Removal in SAR Image Processing," *J. Med. Syst.*, vol. 43, no. 7, p. 222, Jun. 2019. doi: 10.1007/s10916-019-1299-0

[26] S. Chen and L. Mei, "Structure similarity virtual map generation network for optical and SAR image matching," *Frontiers in Physics*, vol. 12, p. 1287050, 2024. doi: 10.3389/fphy.2024.1287050

[27] S. Jiao and W. Dong, "SAR image quality assessment based on SSIM using textural feature," in *Proc. 7th Int. Conf. Image and Graphics (ICIG)*, 2013, pp. 281–286. doi: 10.1109/ICIG.2013.62

[28] U. Sara, M. Akter, and M. S. Uddin, "Image Quality Assessment through FSIM, SSIM, MSE and PSNR—A Comparative Study," *J. Comput. Commun.*, vol. 7, no. 3, pp. 8–16, Mar. 2019. doi: 10.4236/jcc.2019.73002

[29] V. Geetha and S. K. Narayanan, "Laplacian pyramid based speckle reducing anisotropic diffusion (LPSRAD) for SAR images," *Int. J. Appl. Eng. Res.*, vol. 10, pp. 22702–22707, 2015.

[30] V. Jain, S. Shitole, and M. Rahman, "Performance evaluation of DFT based speckle reduction framework for synthetic aperture radar (SAR) images at different frequencies and image regions," *Remote Sens. Appl.: Soc. Environ.*, vol. 31, p. 101001, 2023. doi: 10.1016/j.rsase.2023.101001

[31] V. Jain, S. Shitole, V. Turkar, and A. Das, "Impact of DFT based speckle reduction filter on classification accuracy of synthetic aperture radar images," in *Proc. InGARSS*, 2020. doi: 10.1109/InGARSS48198.2020.9358943

[32] V. Jain, S. Shitole, M. Rahman, and A. Dhruv, "Evaluating the Impact of DFT based Speckle Reduction Filter on T3 Matrix Elements in Polarimetric SAR Imagery," *Research Square*, Aug. 16, 2024. doi: 10.21203/rs.3.rs-4748058/v1

[33] V. Turkar et al., "MATSAR: A comprehensive machine learning approach for PolSAR data processing," *Int. J. Comput. Appl.*, vol. 187, no. 3, pp. 23–29, May 2025. doi: 10.5120/ijca2025924824

[34] W. M. Laghari, M. U. Baloch, M. A. Mengal, and S. J. Shah, "Performance Analysis of Analog Butterworth Low Pass Filter as Compared to Chebyshev Type-I Filter, Chebyshev Type-II Filter and Elliptical Filter," *Circuits and Systems*, vol. 5, no. 9, pp. 228–234, Sep. 2014. doi: 10.4236/cs.2014.59023

[35] X. Zhao, F. Ren, H. Sun, and Q. Qi, "Synthetic Aperture Radar Image Despeckling Based on a Deep Learning Network Employing Frequency Domain Decomposition," *Electronics*, vol. 13, no. 3, p. 490, 2024. doi: 10.3390/electronics13030490

[36] Z. Ge, H. Guo, T. Wang, et al., "Universal graph filter design based on Butterworth, Chebyshev, and elliptic functions," *Circuits, Systems, and Signal Processing*, vol. 42, pp. 564–579, Jan. 2023. doi: 10.1007/s00034-022-02145-w